Chapter 7
Carbon-Based Nanomaterials for Oxygen Evolution Reaction

Mengli Liu, Siran Xu, and Bang-An Lu

Abstract The oxygen evolution reaction (OER), one of the semi-reactions of water electrolysis, is expected to play an important role in the conversion and storage of energy in the future. The sluggish four-electron transfer reaction has become the primary bottleneck of electrochemical water splitting, which can be significantly alleviated with the development of low-cost and durable OER catalysts, fortunately. Carbon-based composite nanomaterials can function well in alkaline environments because of their excellent mechanical and electrical properties, low cost, high abundance, and large surface area. This chapter discusses recent breakthroughs in carbon-based OER electrocatalysts, mainly including metal-free catalysts, atomically dispersed metallic carbon, metal-encapsulated carbon nanoparticles, and carbon nanoparticles supported by metal nanoparticles. The knowledge offered in this chapter can be used to rationally design OER carbon-based composite nanomaterial catalysts, which may help shed light on the future of carbon-based OER development.

7.1 Introduction

In recent years, with the increase of the global population, the total energy demand has increased rapidly, leading to excessive consumption of traditional fossil energy and accompanied by increasingly serious environmental pollution problems [1, 2]. As a result, the urgent need for new energy forms and carriers, as well as the desire to reduce long-term excessive reliance on fossil energy, researchers in energy-related

M. Liu · S. Xu · B.-A. Lu (✉)
College of Materials Science and Engineering, Zhengzhou University, Zhengzhou 450001, P. R. China
e-mail: balu@zzu.edu.cn

M. Liu
e-mail: 13592573680@163.com

S. Xu
e-mail: siranxuhbnu@163.com

J.-N. Zhang (ed.), *Carbon-Based Nanomaterials for Energy Conversion and Storage*, Springer Series in Materials Science 325, https://doi.org/10.1007/978-981-19-4625-7_7

fields are exploring and developing environmentally friendly and sustainable new energy and production technologies. In order to achieve the goal of carbon neutrality and find alternatives to renewable energy and clean energy, such as wind energy, tidal energy, solar energy, and geothermal energy, a lot of efforts have been made [3, 4]. However, due to the lack of suitable energy storage technology, these intermittent energy sources cannot be widely used [5, 6]. Hydrogen energy has significant advantages as a zero-carbon energy source. Because of its high energy density, H_2 can be used to store large amounts of energy indefinitely. Low-pollution fuel cells can then be used to regenerate the electrical energy. Additional to this, the high-value-added chemicals can also be produced by using H_2 [7–9]. Fossil fuels, biomass, and water splitting are the three primary sources of hydrogen production currently available. However, hydrogen production from fossil fuels and biomass involves the use of limited fossil energy, resulting in environmental contamination. Electrochemical water splitting to produce hydrogen is therefore expected to become the primary method of producing hydrogen because of its durability and low pollution [10–12].

The electrocatalytic water splitting is the reverse process of the fuel cell reaction, including the hydrogen evolution reaction (HER) at the cathode and the oxygen evolution reaction (OER) at the anode [13–15]. Both of these reactions require efficient catalysts to accelerate the reaction kinetics. HER is a relatively simple two-electron transport process involving electrochemical H^+ adsorption and H_2 desorption. In contrast, the OER process involves a complex four-electron-proton coupling process. Due to its slow kinetic reaction, it becomes a bottleneck for the production of hydrogen by electrochemical water splitting [16]. Meanwhile, OER is also an important semi-response of rechargeable metal-air batteries. However, due to the inherent slow kinetics of OER, the metal-air battery has low life, low energy conversion efficiency, and limited stability [17]. The reaction path of OER process in acidic and alkaline electrolytes is shown in the following formula:

Acid:

$$H_2O\,(l) + {}^* \rightarrow OH^* + \left(H^+ + e^-\right) \tag{7.1}$$

$$OH^* \rightarrow O^* + \left(H^+ + e^-\right) \tag{7.2}$$

$$O^* + H_2O(l) \rightarrow OOH^* + \left(H^+ + e^-\right) \tag{7.3}$$

$$OOH^* \rightarrow {}^* + O_2(g) + \left(H^+ + e^-\right) \tag{7.4}$$

Alkaline:

$$OH^- + * \rightarrow OH * + e^- \tag{7.5}$$

$$OH^* + OH^- \rightarrow O^* + H_2O(l) + e^- \tag{7.6}$$

$$O^* + OH^- \rightarrow OOH^* + e^- \tag{7.7}$$

$$OOH^* + OH^- \rightarrow {}^* + O_2(g) + H_2O(l) + e^- \tag{7.8}$$

In the formula, (l) and (g) are gas and liquid phases, respectively, * is the active site on the catalyst, and O*, OH*, OOH* are adsorption intermediates.

The OER can be divided into four steps. Each step involves the transfer of an electron. The overpotential of OER can be determined by the free energy of the reaction of all four steps [18]. The energy barriers of different reaction intermediates are related to the catalyst's electronic structure and interface structure. This basic identification of OER mechanism and activity source is a prerequisite for designing advanced OER electrocatalysts [19, 20].

Generally speaking, there are two possible mechanism for the OER process, one is the traditional adsorbate evolution mechanism (AEM), and the other is the lattice oxygen mediated mechanism (LOM) [21–23]. AEM is considered to be a conventional OER mechanism. AEM involves four proton-coupled electron transfer processes centered on metal ions. The source of oxygen is mainly water molecules adsorbed in the electrolyte. Specifically, first, water molecules are adsorbed on the surface of the metal site through a single-electron oxidation process, forming an adsorbed *OH on the metal site (*). Then *OH forms *O species through proton coupling and electron removal. Another water molecule is adsorbed to form the *OOH intermediate in the next step. Finally, *OOH is oxidized, releasing O_2, and the original clean metal active sites are restored. On the scale of reversible hydrogen electrodes, AEM usually produces activity independent of pH. However, LOM clearly pointed out the necessity of considering the surface of the dynamic catalyst, and the active sites on the surface of the dynamic catalyst are not limited to the metal center. The LOM concept involving the reaction of lattice oxygen was first proposed by Damjanovic and Jovanovic in 1976 [24]. In late 2015, Binninger et al. [25] proposed a more formal description and coined the term for the lattice oxygen evolution reaction in a typical LOM [25]. LOM involves the participation of lattice oxygen in the electrocatalyst, and oxygen is generated by lattice oxygen atoms. The first two steps are similar to those in AEM. However, in the third step, the adsorbed *O couples with the lattice oxygen on the electrocatalyst, releasing an oxygen molecule and leaving an oxygen vacancy. In order to produce adsorbed *H, the fourth step is supplemented with water and dissociated. The final deprotonation results in a clean metal site. Electrocatalyst electronic structure can be controlled by LOM's OER mechanism, which is based on LOM's metal–oxygen covalent bond [26].

The catalyst plays a critical role in accelerating the reaction rate and increasing the selectivity/efficiency of the OER. As a result, theoretical and experimental research on the design and development of effective and stable OER catalysts is still an important area of study. Despite being the most advanced OER electrocatalysts, IrO_2 and RuO_2 are not widely used because of their high cost and limited availability. In order to develop low-cost OER electrocatalysts with high activity and high stability, a great deal of work has been done thus far. For example, nitrides, phosphides,

sulfides, and selenides have been investigated as alternative OER electrocatalysts [27–32]. Carbon-based composites have shown surprising advantages in OER in recent years, including the acceptable cost of carbon matrix, the structural diversity provided by carbon-based composites, good electrical and thermal conductivity, and mechanical strength and lightness that traditional materials cannot match [33]. It also has a wide range of compositions and good conductivity, thanks to the addition of heteroatoms. The electrode becomes more stable when oxygen escapes thanks to this combination (bubble formation) [34]. Therefore, carbon-based nanocomposites have great potential in catalyzing OER.

OER carbon-based catalysts will be detailly introduced in this chapter including metal nanoparticle/alloy, atom dispersed metal–carbon, and metal hybrid carbon-based electrocatalysts. A summary of current research of carbon-based OER electrocatalysts in this field is also presented.

7.2 Metal-Free Carbon-Based Electrocatalysts for OER

Noble metals and their oxides, such as palladium, platinum, and RuO_2, IrO_2, are considered the most advanced OER catalysts. Besides, transition metal oxides, hydroxides, metal hybrids, chalcogenide compounds, and other reasonably inexpensive OER electrocatalysts of transition metals and related compounds have been identified based on extensive research. However, these transition metal-based catalysts will undergo oxidation, crystal structure changes, and uncontrolled dissolution when exposed to air or electrolytes. Therefore, in order to obtain high electrocatalytic activity and multifunctional carbon-based metal-free electrocatalyst, different carbon nanostructures are often doped with other heteroatoms and defect engineering, such as nitrogen (N), boron (B), sulfur (S), phosphorus (P), and fluorine (F) [35–39]. These may change the electronic structure of carbon materials and become active sites for catalytic reactions, although other factors affect electrocatalytic activity. The charge transfer efficiency of catalysts depends on various factors, such as specific surface area, number of active centers, conductivity, adsorption energy of intermediate products, and electrolyte stability.

In this context, carbon-based metal-free electrocatalysts for ORR have come a long way since their discovery in 2009 [40, 41]. Carbon-based metal-free electrocatalysts as a substitute for noble metal-based electrocatalysts have been widely researched to be effective OER catalysts [35, 42]. In 2013, it is reported for the first time that N-doped porous carbon prepared from melamine formaldehyde containing a heteroatom doped can be used as a carbon-based metal-free electrocatalyst (Fig. 7.1a, b), and showed better OER performance than IrO_2 (Fig. 7.1c). The observed OER performance is attributed to the favorable adsorption of positively charged C atoms by OH^- ions generated by charge transfer induced by adjacent N doping. Experimental and theoretical studies have also shown that the high oxygen evolution activity of

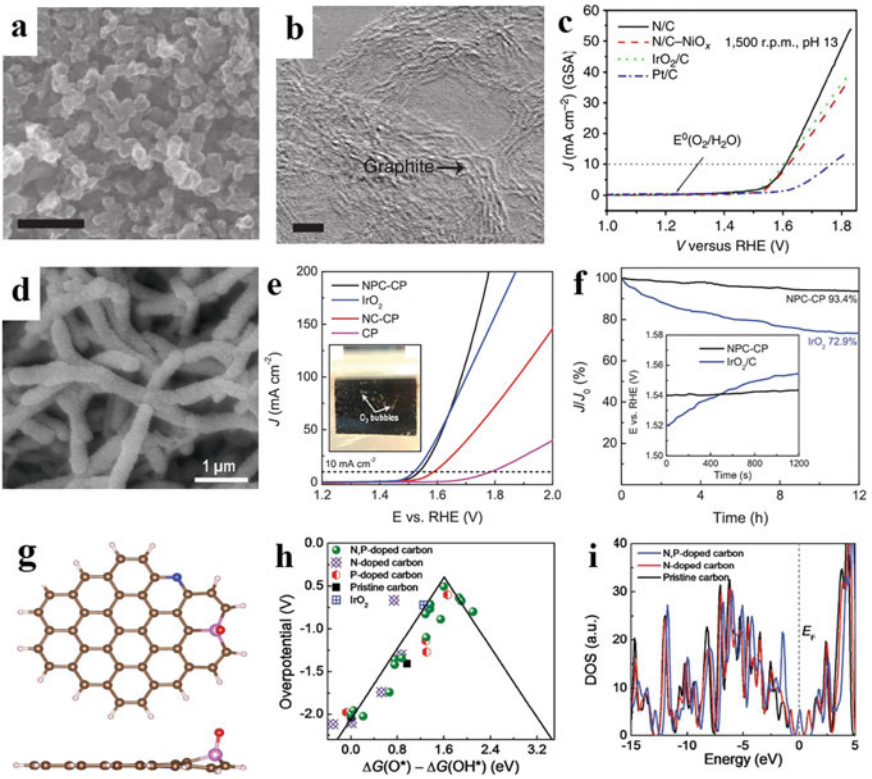

Fig. 7.1 Metal-free carbon-based electrocatalysts for OER. **a** and **b** The SEM and TEM images of the N/C. **c** Oxygen evolution activities of the N/C, N/C–NiOx, IrO_2/C (20 wt%) and Pt/C (20 wt%) electrodes with KOH electrolyte (pH 13) analysed from RRDE system (loading catalyst: 0.2 mg cm^{-1}; rotation speed: 1500 r.p.m.; and scan rate: 5 mV s^{-1}) [35]. Copyright 2013, Nature Publishing Group. **d** SEM image of NPC–CP. **e** OER curves of NPC–CP, NC–CP, IrO_2, and pristine CP in O_2-saturated 1 M KOH (scan rate: 2 mV s^{-1}). **f** Chronoamperometric responses of NPC–CP and IrO_2 at a constant potential of 1.54 V. Inset in panel **f** shows the corresponding chronopotentiometry response curves with the constant current density held at 10 mA cm^{-2}. **g** Initial structure of N and P co-doped carbons and the corresponding structures. **h** Volcano plots of OER overpotential versus the difference between the adsorption energy of O* and OH*, that is, $\Delta G(O^*) - \Delta G(OH^*)$, for the simulated carbon structures. **i** The DOS for the chemically doped carbon structures [43]. Copyright 2017, WILEY–VCH

nitrogen/carbon materials comes from pyridine nitrogen or/and quaternary-nitrogen-related active sites [35]. The N–P co-doped mesoporous carbon produced by pyrolysis of polyaniline aerogels generated in the presence of phytic acid in 2015 had a high surface area of around 1663 m^2 g^{-1} and shown outstanding electrocatalytic activity in the OER and ORR. It is also attractive advantages after being used in zinc-air batteries. After mechanical charging, the two-electrode rechargeable battery is stable for up to 240 h and 180 cycles at 2 mA cm^{-2}. Its maximum power density is 55 mW cm^{-2}. In terms of alkaline electrolytes, it is comparable to commercial

metal air batteries. For chemical species' adsorption and catalytic activity, density functional theory (DFT) calculations show that a distance between the doping site and the edge of the carbon structure appears to be critical. For ORR and OER to function in both modes, a high-porosity foamed carbon network and N/P heteroatom co-doping are required [42]. Coincidentally, multi-stage porous N/P co-doped carbon nanofibers were immediately produced on conductive carbon paper by electrochemically induced polymerization in the presence of aniline monomer and phosphonic acid. (Fig. 7.1d). The synthesized material has stable stability (the activity decays little after 12 h of continuous operation) and high activity (Fig. 7.1e, f). Through DFT calculations, a model of double doping of N and P heteroatoms was constructed (Fig. 7.1g), and it was found that the P doping at the edge is more conducive to the precipitation of oxygen than the P dopant at the center. From a thermodynamic point of view, the ideal catalyst is the lower the overpotential, the better the catalytic performance. From the volcano plots of overpotential versus the difference between the adsorption energy of O* and OH* on the carbon nanostructures, it can be seen that N, P-doped carbon has the smallest overpotential (0.505 V) (Fig. 7.1h), even better than IrO_2. In addition, according to the density of states (DOS) (Fig. 7.1i), the N, P-doped carbon exhibits metallic properties with a relatively higher DOS crossing the Fermi level (E_F), which indicates that the electron transfer capability is improved and the charge distribution is optimized. Theoretically verified the effectiveness of the co-doping of N and P atoms in the collaborative creation of OER active sites and the improvement of the electronic conductivity of the carbon network [43]. Due to the effectiveness of heteroatom doping, carbon materials co-doped with three heteroatoms have been studied. By thermally activating a mixture of polyaniline-coated graphene oxide and ammonium hexafluorophosphate (AHF), a multifunctional electrocatalyst constituted of graphene doped with nitrogen, phosphorus, and fluorine is generated. The gas from the thermal decomposition of AHF promotes the formation of a template-free porous structure. The synthesized N, P, and F three-doped graphene exhibit good electrocatalytic activity for ORR, OER, and HER. It is further used as an OER-HER dual-function catalyst for oxygen and hydrogen production in an electrochemical water splitting device. The device is powered by an integrated Zn-air battery based on an air electrode made of the same ORR electrocatalyst. Therefore, low-cost metal-free trifunctional electrocatalysts have broad application prospects [39].

Carbon-based metal-free electrocatalysts can also benefit from construction defect engineering in addition to heteroatom doping. Nitrogen-doped ultra-thin carbon nanosheets (NCNs) can be made by pyrolyzing a citric acid and NH_4Cl mixture and then using a spontaneous gas foaming method. Ultra-thin sheet structure, ultra-high specific surface area (1793 $m^2\ g^{-1}$), abundant edge defects, low overpotential, and stable ORR, OER and HER properties were achieved by synthesizing NCN-1000–5. Its high energy density, low charge/discharge voltage gap, high reversibility, and long cycle stability all come from the zinc-air rechargeable battery's use of NCN-1000–5 as the cathode catalyst. In ORR, OER, and HER, it is determined that the intrinsic active sites are the carbon atoms on the armchair's edge and adjacent graphite N dopants, thanks to DFT calculations [44].

7.3 Atomically Dispersed Metal Carbon-Based Electrocatalysts for OER

In recent years, the research on isolated metal atoms has increased dramatically, which has aroused widespread scientific interest in the new frontier field of atomic-level dispersion catalysis. The atomically dispersed active sites usually exhibit the most excellent catalytic activity [45]. In contrast to nanoparticle catalysts, atomically dispersed catalysts typically contain positively charged monodisperse metal atoms and coordination sites devoid of metal–metal bonds of the same metal. However, reducing the size of a metal particle to a single atom increases its surface free energy, making it easy to aggregate or Ostwald ripening. Therefore, it is necessary to anchor and strongly bond atomically dispersed metal atoms on a suitable carrier [46]. Carbon-based materials have proven to meet this need because they provide a large surface area. Metal ions can be stabilized on the carbonaceous carrier by forming ions or covalent bonds with heteroatoms (C, N, S, and P), thereby overcoming high aggregation tendency. Unique catalytic mechanisms, including electron transfer pathways or interactions with reactants, intermediaries, and products, are made possible by the singular electronic and geometric properties of the single atom (SAC). Scientific research and industrial applications have paid close attention to the unique properties and catalytic performance of atomic-level dispersion catalysts. As summarized in some excellent review articles [47, 48] the characterization of atomic-level dispersion catalysts is mainly based on some modern atomic resolution techniques, such as aberration-corrected high-angle circular dark-field scanning transmission electron microscopy (AC-HAADF-STEM). To identify scattered metal atoms on a carbon substrate, [49] X-ray absorption spectroscopy (XAS) is also useful, X-ray absorption near edge structure (XANES) provides information on the oxidation state of metal atoms, and extended X-ray absorption fine structure (EXAFS) technology provides detailed information about the coordination structure [50]. In addition, advanced theoretical modeling and simulation methods can build a reliable model for the active site to simulate the catalytic cycle [51]. The dispersed metal carbon-based electrocatalysts discussed in this chapter are typically formed of isolated atoms and carbon support materials that attach, restrict, or coordinate with isolated metal atoms.

The design and manufacture of isolated metal atoms as heterogeneous catalytically active substances can be traced back to 1995, which Thomas and colleagues reported that an oxygen-coordinated Ti SAC was used in the epoxidation reaction of cycloolefins [52]. The complex is grafted onto mesoporous silica and then calcined to synthesize. Until 2011, Zhang et al. [53] used the co-precipitation method to fix atomic Pt on the FeOx carrier and proposed the concept of single-atom catalysis for the first time. Since then, researchers' scientific interest in single atoms has increased dramatically, and atomic-level dispersed metal–carbon-based catalysts have entered a new stage of development.

In an earlier study, Jahan et al. [54] described the OER activity of Cu SAC in GO-MOF. Ding et al. [55] developed a sandwich structure in which a uniform polymer

ionic liquid (PIL) is coated on the surface of carbon nanotubes, and Co atoms are dispersed on the interface (Fig. 7.2a, b). In terms of electrochemical performance, the OER catalytic activity of CoSSPIL/CNT is significantly better than Co_3O_4/CNT

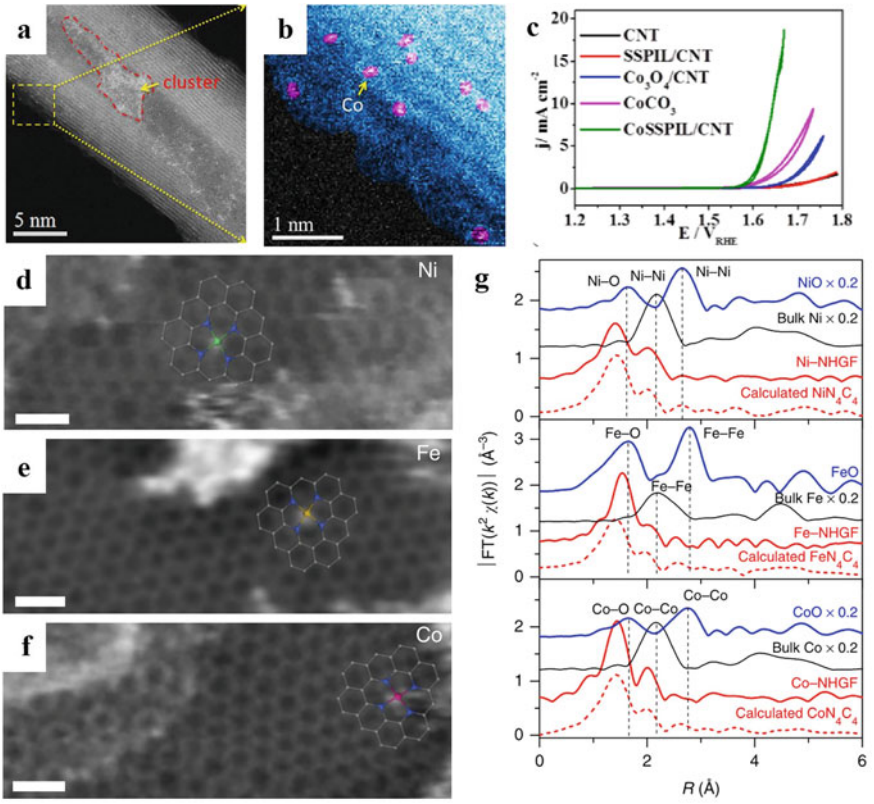

Fig. 7.2 Atomically dispersed metal carbon-based electrocatalysts for OER. **a** and **b** ADF-STEM images of the CoSSPIL/CNT. **c** CV of different samples normalized to the geometric area of the active electrode area [55]. Copyright 2017, WILEY–VCH. High-resolution TEM images enable the direct visualization of the atomic metals of **d** Ni, **e** Fe, and **f** Co embedded in the 2D graphene lattice. The overlaid schematics represent the structural models determined from XAFS analysis. Scale bars, 0.5 nm. The bright region at the top part of d is attributed to out-of-focus thick graphene layers or non-planar flakes. **g** Fourier transformed magnitudes of the experimental K-edge EXAFS signals of M–NHGFs along with reference samples (solid lines). The dashed lines represent calculated spectra based on a divacancy-based MN_4C_4 moiety enclosed in the graphene lattice. The Fourier transforms are not corrected for phase shift. **h** and **i** Proposed reaction scheme with the intermediates having optimized geometry of the single-site (**a**) and dual-site mechanisms (**b**) towards OER. **j** Free energy diagram at 1.23 V for OER over Fe–NHGF, Co–NHGF, and Ni–NHGF with a single-site mechanism, and Ni–NHGF with a dual-site mechanism. The highlights indicate the rate-determining step with the values of the limiting energy barrier labeled. **k** OER activity evaluated by LSV in 1 M KOH at a scan rate of 5 mV s^{-1} for NHGF, Fe–NHGF, Co–NHGF, and Ni–NHGF along with a RuO_2/C catalyst as a reference point. The data are presented with current-resistance (i*R*) correction [56]. Copyright 2018, Nature Publishing Group

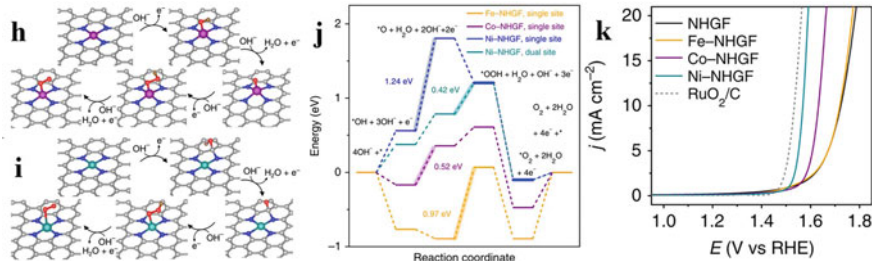

Fig. 7.2 (continued)

and $CoCO_3$ (Fig. 7.2c). In addition, the outstanding electronic conductivity of carbon nanotubes makes it a good carrier for OER. Subsequently, in order to identify the level of activity of different transition metals on OER, Fei et al. [56] reported a method of systematic X-ray absorption fine structure analysis and direct transmission electron microscopy imaging to identify a series of monodisperse atomic transition metals (such as Fe, Co, Ni) are embedded in nitrogen-doped porous graphene frameworks (NHGFs) (Fig. 7.2d–f). This work clearly determined their atomic structure and its correlation with the electrocatalytic activity of OER. Through in-depth analysis of EXAFS and XANES, it is proved that different M-NHGFs adopt the same MN_4C_4 group, have the same local atomic coordination configuration, and are embedded in graphene. In the crystal lattice (Fig. 7.2g). The clear structural configuration of MN_4C_4 allows the use of density functional theory (DFT) to investigate the catalytic performance of M-NHGFs on OER, indicating that the metal's catalytic activity and mechanism path are strongly dependent on the d orbital configuration. The activity trend is inversely proportional to the d orbital configuration, namely Ni-NHGF > Co–NHGF > Fe–NHGF (Fig. 7.2h–j). Electrochemical tests have further confirmed this (Fig. 7.2k). Determining the atomic structure and its correlation with catalytic performance is a key step for the rational design and synthesis of noble metals or non-precious metal SACs with extremely high atom utilization and catalytic activity.

Since then, the transition metal Ni has been favored by researchers. Hou et al. [57] reported an electrocatalyst in which atom-dispersed nickel coordinated with nitrogen and sulfur in porous carbon nanosheets (S|NiNx–PC), which showed excellent activity and durability, even better than the commercial Ir/C. Theoretical and experimental results show that the well-dispersed S|NiNx species serves as the active site of OER. This unusual electrocatalytic activity is derived from the optimized density of states distribution of the S|NiNx center and the enhanced electron transfer capability spectrum measurement, which synergistically promotes the oxidation kinetics, according to experimental observations and theoretical calculations. Zhang et al. [58] reported a simple method to construct a hollow carbon matrix decorated with isolated nickel and N atoms (HCM@Ni–N). Combining experimental and theoretical methods revealed that effective electronic coupling through Ni–N

coordination is the key to regulating the OER mechanism. Precisely, the electronic coupling can significantly move the Fermi level downward, which may substantially impact the adsorption of the intermediate and the final OER kinetics. The new Ni–OG SACs developed by Li et al. [59] have a three-dimensional porous framework, a two-dimensional (2D) ultra-flaky structure, a single Ni atom uniformly distributed, a suitable Ni–O coordination, a significant activating effect on OER, and outstanding activity and durability.

Although some single-atom OER catalysts have been reported, [54–59] bimetallic catalysts with secondary metal introduction are generally more active than single-metal catalysts. Bai et al. [60] reported a cobalt-iron diatomic catalyst (Co–Fe–N–C), which was generated from atomically dispersed Co pre-catalyst (Co–N–C) by an in-situ electrochemical method in an iron-containing alkaline electrolyte. Compared with Co–N–C, Fe is necessary to enhance the activity of Co–Fe–N–C, and the former's activity increases with the increase of Fe content. Operando XAS data shows that Co–N–C undergoes significant structural changes after being immersed in an alkaline electrolyte, and Fe is incorporated in the electrochemical activation process to form a dimer Co–Fe structural element, which is the active site of OER. Han et al. [61] proposed a strategy for preparing heteroatom-doped bimetallic single-atom catalysts. Pyrolysis was used to create N-doped hollow carbon nanocubes (CoNi-SAs/NC) with atomically dispersed double Co–Ni sites using the dopamine-coated metal–organic framework (MOF) as a template. The atomically isolated bimetallic configuration in CoNi–SAs/NC was identified using a combination of microscopy and spectroscopy techniques. When used as an oxygen electrocatalyst in an alkaline medium, the resulting CoNi–SAs/NC hybrid material exhibits excellent catalytic performance in dual-function ORR/OER, which improves the efficiency of a realistic rechargeable zinc-air battery. According to theoretical calculations based on density functional theory, the synergistic effect of uniformly dispersed single atoms and adjacent Co–Ni bimetallic centers can optimize adsorption/desorption characteristics, reduce overall reaction barriers, and ultimately promote reversible oxygen electrocatalysis. This research provides ideas for the controlled synthesis of atomically isolated advanced materials. These research results will guide the further rational design and preparation of SACs with multiple active sites and a deep understanding of synergistic effects in energy-related catalysis applications.

7.4 Metal Nanoparticles Encapsulated Carbon-Based Electrocatalysts for OER

Transition metal (TM)-based electrocatalysts in OER face two major challenges: poor efficiency and unstable performance. It is possible to use nanoparticles made of TM encapsulated in carbon-based materials, which are stable against dissolution under operating conditions and prevent the agglomeration of small metal fragments [62]. In addition, the carbon shell's good electrical conductivity and high porosity

make it easier for electrons and electrolytes to move through the material. As a result, it is believed that the core structure of the transition metal particles influences the electronic structure of the thin carbon shell layer, thereby increasing its OER [18, 63]. The electronic effect of the metal-based core is dependent on the thickness of the graphite layer, which is worth noting. This effect will be reduced if the carbon layer is too thick. For carbon/transition metal composite catalysts, core–shell composite structure (i.e. carbon encapsulation) provides synergistic effect. Encapsulated metal nanoparticle carbon-based catalysts are discussed, as are the difficulties and opportunities currently facing this field.

Liang et al. [64] prepared a novel multilayer bent onion-like carbon nanosphere coated Co–N-C electrocatalyst (OLC/Co–N-C) by pyrolysis of surfactant P123-coated ZIF-67 precursor. With the addition of surfactant micelles, it was demonstrated that the mesoporous/microporous structure formed by the OLC/Co–N–C material during pyrolysis has a large electrochemical surface area and a high concentration of active sites. Due to the interaction of electronic and nanostructural effects, the OLC/Co–N–C catalysts exhibit superior ORR/OER performance ($E_{1/2} = 0.855$ V in 0.1 M KOH, $\eta_{10} = 344$ mV in 1.0 M KOH) and Zn-air battery performance (small charge/discharge voltage gap: 0.8 V at 2 mA cm^{-2}), as well as long-term cycling stability (>100 h). Theoretical calculations explain the experimental results by demonstrating that the curvature of graphitic carbon is critical for the activity of meta-carbon atoms near graphite N and ortho/meta carbon atoms near pyridine N.

In addition to single atoms encapsulated in carbon materials, bimetallic nanoparticles embedded in carbon show similar activity enhancement. Wang et al. [65] successfully developed a simple strategy to control the synthesis of a rare hexagonally sealed (hcp) NiFe nanoparticle (NP) crystal structure encapsulated in a nitrogen-doped carbon (NC) shell (hcp–NiFe@NC). Under alkaline conditions, hcp–NiFe@NC exhibited superior OER activity than the conventional face-centered cubic (fcc) NiFe encapsulated in N-doped carbon shells (fcc-NiFe@NC). When the Fe/Ni ratio is ~5.4%, hcp-NiFe@NC exhibits excellent OER performance, and the NC coating on the NiFe surface also gives it high stability during the OER process. The results indicate that hcp-NiFe NP has good electronic properties, which accelerates the reaction on the NC surface and thus improves the catalytic activity of OER. Besides, Hao et al. [66] reported a novel method to prepare FeCo alloy nanoparticles (NPs) embedded with N, P co-doped carbon encapsulated N-doped carbon nanotubes (NPC/FeCo@NCNTs), where the NCNTs were derived from graphene oxide (GO) nanosheets and melamine. Specifically, the melamine-GO–PS–Fe–Co composites were obtained by strong complex interactions (e.g., electrostatic interactions, covalent and coordination bonds) between melamine, GO, PS (polystyrene spheres), $FeCl_3$, and $Co(NO_3)_2$. N-doped carbon nanotubes embedded with FeCo NPs (FeCo@NCNT) were generated by two-step calcination of the melamine-GO–PS–Fe–Co composites. The formation of NPC/FeCo@NCNT was achieved by calcination of FeCo@NCNT in polyphosphazenes (Fig. 7.3a, b). Interestingly, the electrocatalytic performance of NPC/FeCo@NCNT was greatly enhanced when it was used as a bifunctional catalyst for ORR and OER. In particular, the overpotential of NPC/FeCo@NCNT only needs 339.5 mV can provide a current density of

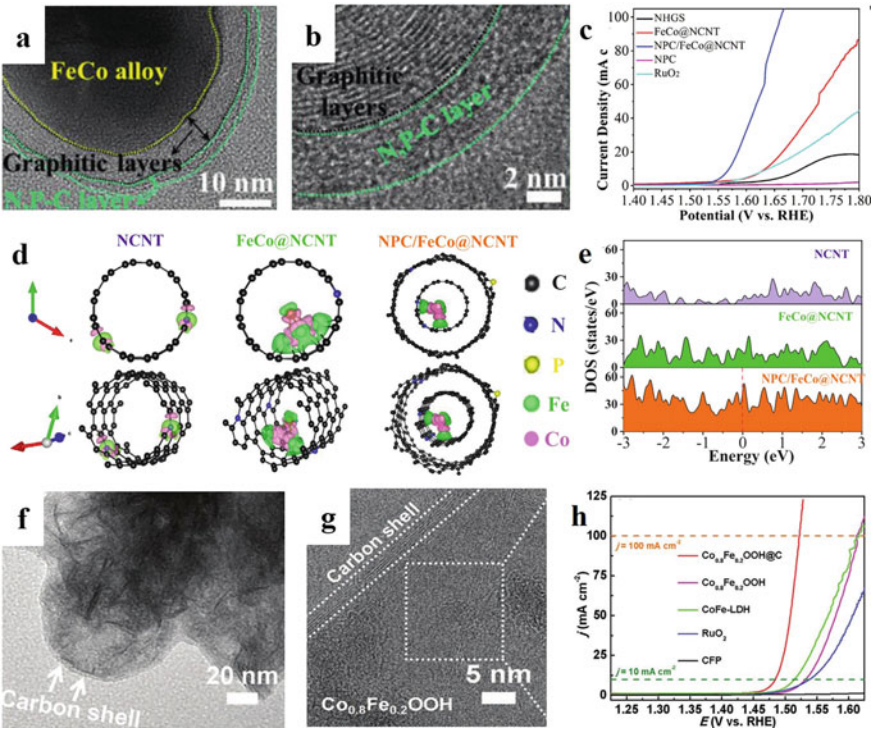

Fig. 7.3 Metal nanoparticles encapsulated carbon-based electrocatalysts for OER. **a** and **b** TEM images of NPC/FeCo@NCNT. **c** OER polarization curves of NHGS, FeCo@NCNT, NPC/FeCo@NCNT, NPC, and RuO_2 in 0.1 M KOH. **d** The optimized geometry models and **e** the calculated density of states of NCNT, FeCo@NCNT, and NPC/FeCo@NCNT [66]. Copyright 2021, WILEY–VCH. **f** TEM image and **g** HR-TEM image of the amorphorized $Co_{0.8}Fe_{0.2}OOH$@C nanosheets. **h** Polarization curves of $Co_{0.8}Fe_{0.2}OOH$@C nanosheets, $Co_{0.8}Fe_{0.2}OOH$, CoFe–LDH nanosheets, commercial RuO_2, and the CFP substrate at a scan rate of 5 mV s^{-1} in 1.0 M KOH [67]. Copyright 2020, WILEY–VCH

10 mA cm^{-2} for OER (Fig. 7.3c) and shows an onset potential of 0.92 V to drive ORR. More impressively, the bifunctional activity parameter (ΔE) of NPC/FeCo@NCNT is as low as 0.741 V, indicating that its bifunctional catalytic activity is better than most of the reported state-of-the-art bifunctional electrocatalysts. Three geometrical configurations, NCNT, FeCo@NCNT, and NPC/FeCo@NCNT, were constructed by density flooding theory (DFT) to simulate the occurring OER/ORR process (Fig. 7.3d). Figure 7.3e shows that all catalysts exhibit an ideal density of states, all above the Fermi energy level, indicating the high conductivity of these catalysts. The electronic states near the Fermi energy level of FeCo@NCNT are enhanced compared to those of NCNT, indicating the improved metallic character of the material. The metallic character of NPC/FeCo@NCNT can be enhanced due to the hybridization effect between the 2p state of the N atom and the adjacent C atom and the 3d state of the FeCo atom, resulting in a sharper peak near the Fermi energy level. The charge

distribution analysis shows that the coupling of FeCo clusters to NCNT can achieve direct electron transfer from FeCo to NCNT (Fig. 7.3d). The above analysis indicates that the interaction between FeCo NPs and NCNT and the presence of N and P co-doped carbon structures play an important role in the high catalytic performance of NPC/FeCo@NCNT. Han et al. [67] rationally designed and successfully synthesized efficient electrocatalysts made of amorphous $Co_{0.8}Fe_{0.2}OOH$ nanosheets encapsulated by carbon shells by using $Co_{0.8}Fe_{0.2}P$@C nanosheets as efficient precatalysts (Fig. 7.3f, g). The conversion of cobalt-iron phosphide to the corresponding hydroxide was achieved by in situ electrochemical oxidation and deep structural reconstruction, during which phosphorus species were leached from the phosphide structure, and the residual cobalt-iron species were oxidized. Detailed structural analysis and characterization demonstrate the complete transformation from phosphorylated cobalt-iron to cobalt-iron hydroxide with a bulk phase amorphous structure. Thus, the amorphous $Co_{0.8}Fe_{0.2}OOH$@C nanosheets have highly exposed active sites, abundant edge sites and pores, and an effective conducting framework, which synergistically achieves high oxygen precipitation activity. As a result, only low overpotentials of 254 and 292 mV are required to provide current densities of 10 and 100 mA cm^{-2} (Fig. 7.3h) with excellent stability (15 days of continuous stable operation at 100 mA cm^{-2}). However, in situ studies provide indirect evidence for structural and phase reconstruction during phosphorus leaching, and the origin of the OER active site in $Co_{0.8}Fe_{0.2}OOH$@C nanosheets remains unclear. Therefore, theoretical and in situ/operational conditions analyses are needed as future directions to investigate the mechanism of structural reconstruction and the active catalytic sites on the $Co_{0.8}Fe_{0.2}OOH$ surface. Nevertheless, the present work opens a path for the rational design of amorphous nanomaterials to achieve efficient energy storage/conversion applications.

The activity performance of bimetallic transition metal hybrids encapsulated in carbon materials is also impressive. Cao et al. [68] reported a novel core–shell structure of a binary metal selenide hybrid electrocatalyst consisting of a selenide (cobalt, nickel) core and a nitrogen-doped carbon shell loaded on an electrochemically exfoliated graphite (EG) foil (EG/(Co, Ni)Se_2–NC) on it. The hybrid catalysts were prepared by selenization of CoNi layered double hydroxide (CoNi-LDH)/zeolite imidazolate framework-67 (ZIF-67) nanosheet array. Due to the synergistic effect of the binary metals Co and Ni and N-doped carbon, the EG/(Co, Ni)Se_2–NC hybrid exhibited remarkable OER electrocatalytic performance at a current density of 10 mA cm^{-2} with a low overpotential of 258 mV and a small Tafel slope of 73.3 mV dec^{-1}, which was superior to commercial Ir/C and most reported binary cobalt selenide based materials. In situ electrochemical Raman spectroscopy combined with non-in situ X-ray photoelectron spectroscopy analysis showed that the ultrahigh OER catalytic activity can be attributed to the highly active Co–OOH species and Ni elemental modification of the electron transfer process.

7.5 Metal Nanoparticles Supported Carbon-Based Electrocatalysts for OER

In addition to encapsulating metal nanoparticles in carbon-based materials, they can also be loaded onto carbon-based materials. Xu et al. [69] demonstrated that dual electrical behavior modulation on the electrocatalyst achieved enhanced electrochemical water oxidation. By hybridizing metallic Ni_3C nanoparticles with conductive carbon (Ni_3C/C), the intrinsic metallic properties will promote electron transport within the electrocatalyst phase and the conductive carbon carrier, thus promoting charge transport on the catalyst surface, significantly improving the OER catalytic performance compared to pure Ni_3C, NiO and NiO/C. In addition, the catalytic mechanism of Ni_3C/C was investigated by XAFS characterization, HRTEM, and EELS spectroscopy; the NiOx/Ni_3C/C heterostructure was shown to be an actual effective species for the OER process. Liang et al. [70] reported a hybrid material of Co_3O_4 nanocrystals grown on mild graphene oxide (Fig. 7.4a) as a high-performance bifunctional catalyst for oxygen reduction reaction (ORR) and oxygen precipitation reaction (OER). Although Co_3O_4 or graphene oxide alone has almost no catalytic activity, their hybrids exhibit unexpectedly high ORR activity, which is further enhanced by the nitrogen doping of graphene. The high activity for OER was also observed (Fig. 7.4c), making it a high-performance non-precious metal bi-functional catalyst for ORR and OER. To collect the interactions between CO_3O_4 and GO, X-ray absorption near edge structure (XANES) measurements were performed (Fig. 7.4b).

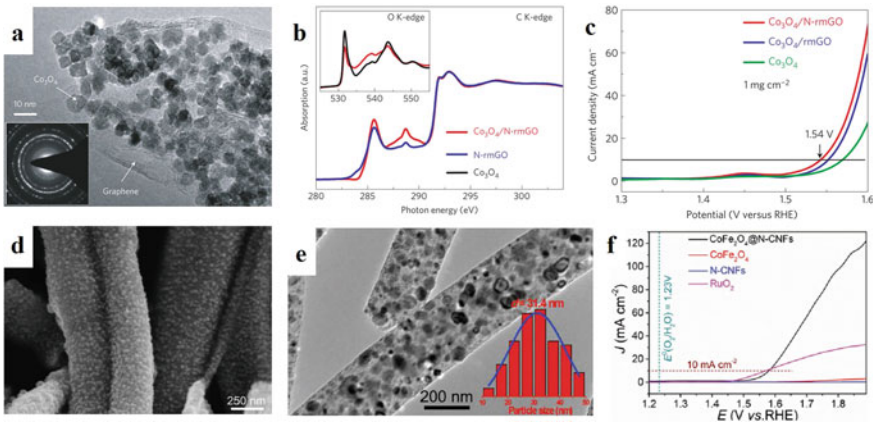

Fig. 7.4 Metal nanoparticles supported carbon-based electrocatalysts for OER. **a** TEM images of Co_3O_4/N–rmGO hybrid. **b** C K-edge XANES of N–rmGO (blue curve) and Co_3O_4/N–rmGO hybrid (red curve). Inset shows O K-edge XANES of Co_3O_4 (black curve) and Co_3O_4/N–rmGO hybrid (red curve). **c** Oxygen evolution currents of Co_3O_4/N–rmGO hybrid, Co_3O_4/rmGO hybrid, and Co_3O_4 nanocrystal loaded onto Ni foam (to reach a high catalyst loading of ~1 mg cm^{-2}) measured in 1 M KOH [70]. Copyright 2011, Nature Publishing Group. **d** and **e** The SEM and TEM images of the obtained $CoFe_2O_4$@N–CNFs. **f** LSV polarization curves of different catalysts [71]. Copyright 2017, WILEY–VCH

bond formation between CO_3O_4 and N-rmGO and changes in the chemical bonding environment of C, O, and Co atoms in the hybrid material may be responsible for the synergistic catalytic activity.

In addition to monometallic nanoparticles, polymetallic nanoparticles loaded on carbon materials are also performed strongly. Li et al. [71] demonstrated a feasible electrostatic spinning method for the simultaneous synthesis of $CoFe_2O_4$ nanoparticles (denoted as $CoFe_2O_4$@N–CNF) uniformly embedded in N-doped carbon nanofibers (Fig. 7.4d–e). By combining catalytically active $CoFe_2O_4$ nanoparticles with N-doped carbon nanofibers, the synthesized $CoFe_2O_4$@N–CNF nanohybrids exhibited excellent OER performance compared to their single-component counterparts (pure $CoFe_2O_4$ and N-doped carbon nanofibers) and commercially available RuO_2 catalysts (Fig. 7.4f). The improved catalytic performance results from the unique one-dimensional structural features and the synergistic interaction between the constituents. Morales et al. [72] reported a highly active OER catalyst $Fe_{0.3}Ni_{0.7}O_x$ using oxygen-functionalized multi-walled carbon nanotubes as a carrier, which was essentially activated as a bifunctional ORR/OER catalyst by the additional addition of MnO_x. Carbon nanotube-loaded trimetallic (Mn–Ni–Fe) oxide catalysts demonstrated extremely low ORR and OER overpotentials. The combination of rare earth-rich transition metal oxides had a strong synergistic effect on catalytic activity. A four-electrode configuration cell assembly comprised an integrated two-layer bifunctional ORR/OER electrode system with each layer dedicated to ORR and OER to prevent the deactivation of ORR activity commonly observed at monolayer bifunctional ORR/OER electrodes after OER polarization was used to evaluate the suitability of the prepared catalysts for reversible ORR/OER electrocatalysis.

7.6 Conclusion and Perspective

Carbon-based OER catalysts have received intense attention in recent years because of their structural and compositional diversity, as well as their good electrocatalytic properties, which have outperformed traditional metal oxide or metal hydroxide electrodes and even noble metals, primarily under alkaline conditions. Although carbon itself does not contribute to these reactions, the high intrinsic OER activity, high possible surface area, and high electrical conductivity provided by the defective and heteroatom-doped structures result in excellent OER activity with low overpotential. The transition metals-doping can further boost carbon activity. Encasing metal or metal compound particles in thin graphite layers or nanotube structures is another strategy. The metal core's electronic effects can activate the carbon layer for OER. In general, these core–shell layer materials are more active than doped carbon (except for atomically dispersed materials).

Despite the exciting advances of carbon-based OER catalysts, there are still some challenging questions to be answered:

(1) It is blurry for the real active sites and reaction mechanisms of various carbon-based materials. High-resolution in situ microscopy and spectroscopic techniques combined with advanced theoretical calculations (i.e., considering electrolytes and potentials) may help fully understand the role of doped elements and metal/metal compound cores.
(2) Increasing the number of active sites is also an effective strategy to enhance OER performance. For example, the metal atom loading is very low for atomically dispersed catalysts. Increasing the metal loading while maintaining atomic dispersion is a challenging task. More advanced synthesis methods need to be developed.
(3) To better evaluate the activity and stability of carbon-based electrocatalysts, the assessment of industrial electrolytic cell parameters is necessary. To date, almost all evaluation data are based on liquid cell test reports and may not represent the electrolytic cell's actual performance. The viability of carbon-based materials as anode and cathode catalysts should be evaluated in the industrial electrolytic cell. The results of such tests are essential to guide the future development of carbon-based electrocatalysts.
(4) Development of in-situ characterization. Most transition metal-based catalysts undergo phase changes under OER conditions, including structure, valence state, and coordination environment. Most of the research works have used non-in situ techniques, which can only give the characterization results before and after OER measurements. However, the basic origin of the structural evolution information and self-reconstruction during OER is not fully understood. Therefore, the use of in situ techniques to detect intermediates and their adsorption/desorption behavior is essential to obtain direct experimental evidence for the proposed OER mechanism. The combination of in situ techniques, theoretical calculations, and electrochemical measurements can more effectively reveal the reaction mechanism and guide the rational design of optimized OER electrocatalysts.
(5) Balancing the cost, stability, and universality of materials. Low cost, including synthetic feedstock and manufacturing process and robust stability, can be effectively operated in commercial facilities for several years. In addition to this, the ability to catalyze OER at a wide range of pH values, especially in acidic media and environmentally neutral electrolytes. However, so far, no OER electrocatalyst has been able to satisfy both of these advantages. Therefore, more efforts should be made in the future.

It provides some case studies for the design and development of new, efficient, low-cost, carbon based OER catalysts, and puts forward some challenges that still exist at present. This provides them with a great opportunity to surpass precious metal based OER catalysts in the clean energy and other technology markets. Continuing research and development in this exciting area will improve fuel economy and reduce the cost of producing important industrial chemicals.

References

1. M.G. Schultz, T. Diehl, G.P. Brasseur, W. Zittel, Air pollution and climate-forcing impacts of a global hydrogen economy. Science **302**, 624–627 (2003). https://doi.org/10.1126/science.1089527
2. Z. Wang, Z. Lin, P. Diao, Hybrids of iridium-cobalt phosphates as a highly efficient electrocatalyst for the oxygen evolution reaction in neutral solution. Chem. Commun. **55**, 3000–3003 (2019). https://doi.org/10.1039/c8cc10278c
3. Z. Yang, J. Zhang, M.C. Kintner-Meyer, X. Lu, D. Choi, J.P. Lemmon, J. Liu, Electrochemical energy storage for green grid. Chem. Rev. **111**, 3577–3613 (2011). https://doi.org/10.1021/cr100290v
4. N.L. Panwar, S.C. Kaushik, S. Kothari, Role of renewable energy sources in environmental protection: A review. Renew. Sustain. Energy Rev. **15**, 1513–1524 (2011). https://doi.org/10.1016/j.rser.2010.11.037
5. B. Li, M.I. Setyawati, H. Zou, J. Dong, H. Luo, N. Li, D.T. Leong, Emerging 0D transition-metal dichalcogenides for sensors, biomedicine, and clean energy. Small **13**, 1700527 (2017). https://doi.org/10.1002/smll.201700527
6. C. Le Quéré, M.R. Raupach, J.G. Canadell, G. Marland, L. Bopp, P. Ciais, T.J. Conway, S.C. Doney, R.A. Feely, P. Foster, P. Friedlingstein, K. Gurney, R.A. Houghton, J.I. House, C. Huntingford, P.E. Levy, M.R. Lomas, J. Majkut, N. Metzl, J.P. Ometto, G.P. Peters, I.C. Prentice, J.T. Randerson, S.W. Running, J.L. Sarmiento, U. Schuster, S. Sitch, T. Takahashi, N. Viovy, G.R. van der Werf, F.I. Woodward, Trends in the sources and sinks of carbon dioxide. Nat. Geosci. **2**, 831–836 (2009). https://doi.org/10.1038/ngeo689
7. W. Stedman, H. Kang, S. Lin, J.L. Kissil, M.S. Bartolomei, P.M. Lieberman, The art of splitting water. Nature **27**, 654–666 (2008). https://doi.org/10.1038/451778a
8. J. Song, Z.-F. Huang, L. Pan, K. Li, X. Zhang, L. Wang, J.-J. Zou, Review on selective hydrogenation of nitroarene by catalytic, photocatalytic and electrocatalytic reactions. Appl. Catal. B **227**, 386–408 (2018). https://doi.org/10.1016/j.apcatb.2018.01.052
9. L. Zhang, M. Zhou, A. Wang, T. Zhang, Selective hydrogenation over supported metal catalysts: from nanoparticles to single atoms. Chem. Rev. **120**, 683–733 (2020). https://doi.org/10.1021/acs.chemrev.9b00230
10. N. Ji, T. Zhang, M. Zheng, A. Wang, H. Wang, X. Wang, J.G. Chen, Direct catalytic conversion of cellulose into ethylene glycol using nickel-promoted tungsten carbide catalysts. Angew. Chem. Int. Ed. **47**, 8510–8513 (2008). https://doi.org/10.1002/anie.200803233
11. J.C. Serrano-Ruiz, R. Luque, A. Sepulveda-Escribano, Transformations of biomass-derived platform molecules: From high added-value chemicals to fuels *via* aqueous-phase processing. Chem. Soc. Rev. **40**, 5266–5281 (2011). https://doi.org/10.1039/c1cs15131b
12. S. Yang, Y. Gong, J. Zhang, L. Zhan, L. Ma, Z. Fang, R. Vajtai, X. Wang, P.M. Ajayan, Exfoliated graphitic carbon nitride nanosheets as efficient catalysts for hydrogen evolution under visible light. Adv. Mater. **25**, 2452–2456 (2013). https://doi.org/10.1002/adma.201204453
13. R. Subbaraman, D. Tripkovic, K.C. Chang, D. Strmcnik, A.P. Paulikas, P. Hirunsit, M. Chan, J. Greeley, V. Stamenkovic, N.M. Markovic, Trends in activity for the water electrolyser reactions on 3*d* M(Ni Co, Fe, Mn) hydr(oxy)oxide catalysts. Nat. Mater. **11**, 550–557 (2012). https://doi.org/10.1038/nmat3313
14. B.M. Hunter, H.B. Gray, A.M. Muller, Earth-abundant heterogeneous water oxidation catalysts. Chem. Rev. **116**, 14120–14136 (2016). https://doi.org/10.1021/acs.chemrev.6b00398
15. C. Spori, J.T.H. Kwan, A. Bonakdarpour, D.P. Wilkinson, P. Strasser, The stability challenges of oxygen evolving catalysts: Towards a common fundamental understanding and mitigation of catalyst degradation. Angew. Chem. Int. Ed. **56**, 5994–6021 (2017). https://doi.org/10.1002/anie.201608601
16. J. Song, C. Wei, Z. Huang, C. Liu, L. Zeng, X. Wang, Z. Xu, A review on fundamentals for designing oxygen evolution electrocatalysts. Chem. Soc. Rev. **49**, 2196–2214 (2020). https://doi.org/10.1039/c9cs00607a

17. H.-F. Wang, Q. Xu, Materials design for rechargeable metal-air batteries. Matter **1**, 565–595 (2019). https://doi.org/10.1016/j.matt.2019.05.008
18. L. Zhang, J. Xiao, H. Wang, M. Shao, Carbon-based electrocatalysts for hydrogen and oxygen evolution reactions. ACS Catal. **7**, 7855–7865 (2017). https://doi.org/10.1021/acscatal.7b02718
19. N.C.S. Selvam, L. Du, B. Xia, P.J. Yoo, B. You, Reconstructed water oxidation electrocatalysts: The impact of surface dynamics on intrinsic activities. Adv. Func. Mater. **31**, 2008190 (2020). https://doi.org/10.1002/adfm.202008190
20. N.T. Suen, S.F. Hung, Q. Quan, N. Zhang, Y.J. Xu, H.M. Chen, Electrocatalysis for the oxygen evolution reaction: recent development and future perspectives. Chem. Soc. Rev. **46**, 337–365 (2017). https://doi.org/10.1039/c6cs00328a
21. X. Rong, J. Parolin, A.M. Kolpak, A fundamental relationship between reaction mechanism and stability in metal oxide catalysts for oxygen evolution. ACS Catal. **6**, 1153–1158 (2016). https://doi.org/10.1021/acscatal.5b02432
22. D.A. Kuznetsov, M.A. Naeem, P.V. Kumar, P.M. Abdala, A. Fedorov, C.R. Muller, Tailoring lattice oxygen binding in ruthenium pyrochlores to enhance oxygen evolution activity. J. Am. Chem. Soc. **142**, 7883–7888 (2020). https://doi.org/10.1021/jacs.0c01135
23. J.H. Montoya, L.C. Seitz, P. Chakthranont, A. Vojvodic, T.F. Jaramillo, J.K. Norskov, Materials for solar fuels and chemicals. Nat. Mater. **16**, 70–81 (2016). https://doi.org/10.1038/nmat4778
24. A. Damjanovic, B. Jovanovic, Anodic oxide films as barriers to charge transfer in O_2 evolution at Pt in acid solutions. J. Electrochem. Soc. **123**, 374–381 (1976). https://doi.org/10.1149/1.2132828
25. T. Binninger, R. Mohamed, K. Waltar, E. Fabbri, P. Levecque, R. Kotz, T.J. Schmidt, Thermodynamic explanation of the universal correlation between oxygen evolution activity and corrosion of oxide catalysts. Sci. Rep. **5**, 12167 (2015). https://doi.org/10.1038/srep12167
26. A. Grimaud, W. Hong, Y. Shao-Horn, J.M. Tarascon, Anionic redox processes for electrochemical devices. Nat. Mater. **15**, 121–126 (2016). https://doi.org/10.1038/nmat4551
27. B. Cao, G.M. Veith, J.C. Neuefeind, R.R. Adzic, P.G. Khalifah, Mixed close-packed cobalt molybdenum nitrides as non-noble metal electrocatalysts for the hydrogen evolution reaction. J. Am. Chem. Soc. **135**, 19186–19192 (2013). https://doi.org/10.1021/ja4081056
28. W. Zhou, J. Zhou, Y. Zhou, J. Lu, K. Zhou, L. Yang, Z. Tang, L. Li, S. Chen, N-doped carbon-wrapped cobalt nanoparticles on N-doped graphene nanosheets for high-efficiency hydrogen production. Chem. Mater. **27**, 2026–2032 (2015). https://doi.org/10.1021/acs.chemmater.5b00331
29. C. Lv, Q. Yang, Q. Huang, Z. Huang, H. Xia, C. Zhang, Phosphorus doped single wall carbon nanotubes loaded with nanoparticles of iron phosphide and iron carbide for efficient hydrogen evolution. J. Mater. Chem. A **4**, 13336–13343 (2016). https://doi.org/10.1039/c6ta04329a
30. S. Fu, C. Zhu, J. Song, M.H. Engelhard, X. Li, D. Du, Y. Lin, Highly ordered mesoporous bimetallic phosphides as efficient oxygen evolution electrocatalysts. ACS Energy Lett. **1**, 792–796 (2016). https://doi.org/10.1021/acsenergylett.6b00408
31. H. Wang, Z. Lu, S. Xu, D. Kong, J.J. Cha, G. Zheng, P.C. Hsu, K. Yan, D. Bradshaw, F.B. Prinz, Y. Cui, Electrochemical tuning of vertically aligned MoS_2 nanofilms and its application in improving hydrogen evolution reaction. Proc. Natl. Acad. Sci. **110**, 19701–19706 (2013). https://doi.org/10.1073/pnas.1316792110
32. S. Sun, Y. Sun, Y. Zhou, S. Xi, X. Ren, B. Huang, H. Liao, L.P. Wang, Y. Du, Z.J. Xu, Shifting oxygen charge towards octahedral metal: a way to promote water oxidation on cobalt spinel oxides. Angew. Chem. Int. Ed. **58**, 6042–6047 (2019). https://doi.org/10.1002/anie.201902114
33. J. Lai, A. Nsabimana, R. Luque, G. Xu, 3D porous carbonaceous electrodes for electrocatalytic applications. Joule **2**, 76–93 (2018). https://doi.org/10.1016/j.joule.2017.10.005
34. W. Xiao, J. Zhu, L. Han, S. Liu, J. Wang, Z. Wu, W. Lei, C. Xuan, H.L. Xin, D. Wang, Pt skin on Pd-Co-Zn/C ternary nanoparticles with enhanced Pt efficiency toward ORR. Nanoscale **8**, 14793–14802 (2016). https://doi.org/10.1039/c6nr03944h
35. Y. Zhao, R. Nakamura, K. Kamiya, S. Nakanishi, K. Hashimoto, Nitrogen-doped carbon nanomaterials as non-metal electrocatalysts for water oxidation. Nat. Commun. **4**, 2390 (2013). https://doi.org/10.1038/ncomms3390

36. L. Yang, S. Jiang, Y. Zhao, L. Zhu, S. Chen, X. Wang, Q. Wu, J. Ma, Y. Ma, Z. Hu, Boron-doped carbon nanotubes as metal-free electrocatalysts for the oxygen reduction reaction. Angew. Chem. Int. Ed. **50**, 7132–7135 (2011). https://doi.org/10.1002/anie.201101287
37. B. Lu, J. Du, T. Sheng, N. Tian, J. Xiao, L. Liu, B. Xu, Z. Zhou, S. Sun, Hydrogen adsorption-mediated synthesis of concave Pt nanocubes and their enhanced electrocatalytic activity. Nanoscale **8**, 11559–11564 (2016). https://doi.org/10.1039/c6nr02349e
38. Z. Liu, F. Peng, H. Wang, H. Yu, W. Zheng, J. Yang, Phosphorus-doped graphite layers with high electrocatalytic activity for the O_2 reduction in an alkaline medium. Angew. Chem. Int. Ed. **50**, 3257–3261 (2011). https://doi.org/10.1002/anie.201006768
39. J. Zhang, L. Dai, Nitrogen, phosphorus, and fluorine tri-doped graphene as a multifunctional catalyst for self-powered electrochemical water splitting. Angew. Chem. Int. Ed. **55**, 13296–13300 (2016). https://doi.org/10.1002/anie.201607405
40. K. Gong, F. Du, Z. Xia, M. Durstock, L. Dai, Nitrogen-doped carbon nanotube arrays with high electrocatalytic activity for oxygen reduction. Science **323**, 760–764 (2009). https://doi.org/10.1126/science.1168049
41. J. Shui, M. Wang, F. Du, L. Dai, N-doped carbon nanomaterials are durable catalysts for oxygen reduction reaction in acidic fuel cells. Sci. Adv. **1**, e1400129 (2015). https://doi.org/10.1126/sciadv.1400129
42. J. Zhang, Z. Zhao, Z. Xia, L. Dai, A metal-free bifunctional electrocatalyst for oxygen reduction and oxygen evolution reactions. Nat. Nanotechnol. **10**, 444–452 (2015). https://doi.org/10.1038/nnano.2015.48
43. Y. Zhu, Y. Jing, A. Vasileff, T. Heine, S. Qiao, 3D dynergistically active carbon nanofibers for improved oxygen evolution. Adv. Energy Mater. **7**, 1602928 (2017). https://doi.org/10.1002/aenm.201602928
44. H. Jiang, J. Gu, X. Zheng, M. Liu, X. Qiu, L. Wang, W. Li, Z. Chen, X. Ji, J. Li, Defect-rich and ultrathin N doped carbon nanosheets as advanced trifunctional metal-free electrocatalysts for the ORR. OER and HER, Energy and Environmental Sciences **12**, 322–333 (2019). https://doi.org/10.1039/c8ee03276a
45. C. Gao, J. Low, R. Long, T. Kong, J. Zhu, Y. Xiong, Heterogeneous single-atom photocatalysts: fundamentals and applications. Chem. Rev. **120**, 12175–12216 (2020). https://doi.org/10.1021/acs.chemrev.9b00840
46. J. Cordon, G. Jimenez-Oses, J.M. Lopez-de-Luzuriaga, M. Monge, The key role of Au-substrate interactions in catalytic gold subnanoclusters. Nat. Commun. **8**, 1657 (2017). https://doi.org/10.1038/s41467-017-01675-1
47. J. Guo, J. Huo, Y. Liu, W. Wu, Y. Wang, M. Wu, H. Liu, G. Wang, Nitrogen-doped porous carbon supported nonprecious metal single-atom electrocatalysts: From synthesis to application. Small Methods **3**, 1900159 (2019). https://doi.org/10.1002/smtd.201900159
48. Y. Chen, S. Ji, C. Chen, Q. Peng, D. Wang, Y. Li, Single-atom catalysts: Synthetic strategies and electrochemical applications. Joule **2**, 1242–1264 (2018). https://doi.org/10.1016/j.joule.2018.06.019
49. J. Hong, C. Jin, J. Yuan, Z. Zhang, Atomic defects in two-dimensional materials: From single-atom spectroscopy to functionalities in opto-/electronics, nanomagnetism, and catalysis. Adv. Mater. **29**, 1606434 (2017). https://doi.org/10.1002/adma.201606434
50. B. Li, C. Zhao, S. Chen, J. Liu, X. Chen, L. Song, Q. Zhang, Framework-porphyrin-derived single-atom bifunctional oxygen electrocatalysts and their applications in Zn-air batteries. Adv. Mater. **31**, e1900592 (2019). https://doi.org/10.1002/adma.201900592
51. L. Cao, Q. Luo, W. Liu, Y. Lin, X. Liu, Y. Cao, W. Zhang, Y. Wu, J. Yang, T. Yao, S. Wei, Identification of single-atom active sites in carbon-based cobalt catalysts during electrocatalytic hydrogen evolution. Nat. Catal. **2**, 134–141 (2018). https://doi.org/10.1038/s41929-018-0203-5
52. T. Maschmeyer, F. Rey, G. Sankar, J.M. Thomas, Heterogeneous catalysts obtained by grafting metallocene complexes onto mesoporous silica. Nature **378**, 159–162 (1995). https://doi.org/10.1038/378159a0
53. B. Qiao, A. Wang, X. Yang, L.F. Allard, Z. Jiang, Y. Cui, J. Liu, J. Li, T. Zhang, Single-atom catalysis of CO oxidation using Pt_1/FeO_x. Nat. Chem. **3**, 634–641 (2011). https://doi.org/10.1038/nchem.1095

54. M. Jahan, Z. Liu, K.P. Loh, A graphene oxide and copper-centered metal organic framework composite as a tri-functional catalyst for HER OER, and ORR. Adv. Funct. Mater. **23**, 5363–5372 (2013). https://doi.org/10.1002/adfm.201300510
55. Y. Ding, A. Klyushin, X. Huang, T. Jones, D. Teschner, F. Girgsdies, T. Rodenas, R. Schlogl, S. Heumann, Cobalt-bridged ionic liquid polymer on a carbon nanotube for enhanced oxygen evolution reaction activity. Angew. Chem. Int. Ed. **57**, 3514–3518 (2018). https://doi.org/10.1002/anie.201711688
56. H. Fei, J. Dong, Y. Feng, C.S. Allen, C. Wan, B. Volosskiy, M. Li, Z. Zhao, Y. Wang, H. Sun, P. An, W. Chen, Z. Guo, C. Lee, D. Chen, I. Shakir, M. Liu, T. Hu, Y. Li, A.I. Kirkland, X. Duan, Y. Huang, General synthesis and definitive structural identification of MN_4C_4 single-atom catalysts with tunable electrocatalytic activities. Nat. Catal. **1**, 63–72 (2018). https://doi.org/10.1038/s41929-017-0008-y
57. Y. Hou, M. Qiu, M.G. Kim, P. Liu, G. Nam, T. Zhang, X. Zhuang, B. Yang, J. Cho, M. Chen, C. Yuan, L. Lei, X. Feng, Atomically dispersed nickel-nitrogen-sulfur species anchored on porous carbon nanosheets for efficient water oxidation. Nat. Commun. **10**, 1392 (2019). https://doi.org/10.1038/s41467-019-09394-5
58. H. Zhang, Y. Liu, T. Chen, J. Zhang, J. Zhang, X.W.D. Lou, Unveiling the activity origin of electrocatalytic oxygen evolution over isolated Ni atoms supported on a N-doped carbon matrix. Adv. Mater. **31**, e1904548 (2019). https://doi.org/10.1002/adma.201904548
59. Y. Li, Z. Wu, P. Lu, X. Wang, W. Liu, Z. Liu, J. Ma, W. Ren, Z. Jiang, X. Bao, High-valence nickel single-atom catalysts coordinated to oxygen sites for extraordinarily activating oxygen evolution reaction. Adv. Sci. **7**, 1903089 (2020). https://doi.org/10.1002/advs.201903089
60. L. Bai, C.S. Hsu, D.T.L. Alexander, H.M. Chen, X. Hu, A cobalt-iron double-atom catalyst for the oxygen evolution reaction. J. Am. Chem. Soc. **141**, 14190–14199 (2019). https://doi.org/10.1021/jacs.9b05268
61. X. Han, X. Ling, D. Yu, D. Xie, L. Li, S. Peng, C. Zhong, N. Zhao, Y. Deng, W. Hu, Atomically dispersed binary Co-Ni sites in nitrogen-doped hollow carbon nanocubes for reversible oxygen reduction and evolution. Adv. Mater. **31**, e1905622 (2019). https://doi.org/10.1002/adma.201905622
62. W. Zhou, T. Xiong, C. Shi, J. Zhou, K. Zhou, N. Zhu, L. Li, Z. Tang, S. Chen, Bioreduction of precious metals by microorganism: efficient gold@N-doped carbon electrocatalysts for the hydrogen evolution reaction. Angew. Chem. Int. Ed. **55**, 8416–8420 (2016). https://doi.org/10.1002/anie.201602627
63. Y. Xu, W. Tu, B. Zhang, S. Yin, Y. Huang, M. Kraft, R. Xu, Nickel nanoparticles encapsulated in Ffew-layer nitrogen-doped graphene derived from metal-organic frameworks as efficient bifunctional electrocatalysts for overall water splitting. Adv. Mater. **29**. https://doi.org/10.1002/adma.201605957
64. Z. Liang, N. Kong, C. Yang, W. Zhang, H. Zheng, H. Lin, R. Cao, Highly curved nanostructure-coated Co, N-doped carbon materials for oxygen electrocatalysis. Angew. Chem. Int. Ed. **60**, 12759–12764 (2021). https://doi.org/10.1002/anie.202101562
65. T. Wang, J. Liang, Z. Zhao, S. Li, G. Lu, Z. Xia, C. Wang, J. Luo, J. Han, C. Ma, Y. Huang, Q. Li, Sub-6 nm fully ordered $L1_0$-Pt-Ni-Co nanoparticles enhance oxygen reduction via Co doping induced ferromagnetism enhancement and optimized surface strain. Adv. Energy Mater. **9**, 1803771 (2019). https://doi.org/10.1002/aenm.201803771
66. X. Hao, Z. Jiang, B. Zhang, X. Tian, C. Song, L. Wang, T. Maiyalagan, X. Hao, Z.J. Jiang, N-doped carbon nanotubes derived from graphene oxide with embedment of FeCo nanoparticles as bifunctional air electrode for rechargeable liquid and flexible all-solid-state zinc-air batteries. Adv. Sci. **8**, 2004572 (2021). https://doi.org/10.1002/advs.202004572
67. X. Han, C. Yu, Y. Niu, Z. Wang, Y. Kang, Y. Ren, H. Wang, H.S. Park, J. Qiu, Full bulk-structure reconstruction into amorphorized cobalt-iron oxyhydroxide nanosheet electrocatalysts for greatly improved electrocatalytic activity. Small Methods **4**, 2000546 (2020). https://doi.org/10.1002/smtd.202000546
68. J. Cao, K. Wang, J. Chen, C. Lei, B. Yang, Z. Li, L. Lei, Y. Hou, K. Ostrikov, Nitrogen-doped carbon-encased bimetallic selenide for high-performance water electrolysis. Nano-Micro Lett. **11**, 67 (2019). https://doi.org/10.1007/s40820-019-0299-4

69. K. Xu, H. Ding, H. Lv, P. Chen, X. Lu, H. Cheng, T. Zhou, S. Liu, X. Wu, C. Wu, Y. Xie, Dual electrical-behavior regulation on electrocatalysts realizing enhanced electrochemical water oxidation. Adv. Mater. **28**, 3326–3332 (2016). https://doi.org/10.1002/adma.201505732
70. Y. Liang, Y. Li, H. Wang, J. Zhou, J. Wang, T. Regier, H. Dai, Co_3O_4 nanocrystals on graphene as a synergistic catalyst for oxygen reduction reaction. Nat. Mater. **10**, 780–786 (2011). https://doi.org/10.1038/nmat3087
71. T. Li, Y. Lv, J. Su, Y. Wang, Q. Yang, Y. Zhang, J. Zhou, L. Xu, D. Sun, Y. Tang, Anchoring $CoFe_2O_4$ nanoparticles on N-doped carbon nanofibers for high-performance oxygen evolution reaction. Adv. Sci. **4**, 1700226 (2017). https://doi.org/10.1002/advs.201700226
72. D.M. Morales, M.A. Kazakova, S. Dieckhöfer, A.G. Selyutin, G.V. Golubtsov, W. Schuhmann, J. Masa, Trimetallic Mn-Fe-Ni oxide nanoparticles supported on multi-walled carbon nanotubes as high-performance bifunctional ORR/OER electrocatalyst in alkaline media. Adv. Func. Mater. **30**, 1905992 (2019). https://doi.org/10.1002/adfm.201905992